Computation of the Standardized Precipitation Index (SPI) and Its Use to Assess Drought Occurrences in Cameroon over Recent Decades

GUY MERLIN GUENANG AND F. MKANKAM KAMGA

Laboratory for Environmental Modelling and Atmospheric Physics, University of Yaoundé 1, Yaoundé, Cameroon

(Manuscript received 16 January 2014, in final form 22 July 2014)

ABSTRACT

The standardized precipitation index (SPI) is computed and analyzed using 55 years of precipitation data recorded in 24 observation stations in Cameroon along with University of East Anglia Climate Research Unit (CRU) spatialized data. Four statistical distribution functions (gamma, exponential, Weibull, and lognormal) are first fitted to data accumulated for various time scales, and the appropriate functions are selected on the basis of the Anderson–Darling goodness-of-fit statistic. For short time scales (up to 6 months) and for stations above 10°N, the gamma distribution is the most frequent choice; below this belt, the Weibull distribution predominates. For longer than 6-month time scales, there are no consistent patterns of fitted distributions. After calculating the SPI in the usual way, operational drought thresholds that are based on an objective method are determined at each station. These thresholds are useful in drought-response decision making. From SPI time series, episodes of severe and extreme droughts are identified at many stations during the study period. Moderate/severe drought occurrences are intra-annual in short time scales and interannual for long time scales (greater than 9 months), usually spanning many years. The SPI calculated from CRU gridded precipitation shows similar results, with some discrepancies at longer scales. Thus, the spatialized dataset can be used to extend such studies to a larger region—especially data-scarce areas.

1. Introduction

Agriculture is the main socioeconomic activity in sub-Saharan African countries. According to Tarhule et al. (2009), about 95% of the used land is devoted to agriculture, which is the main occupation of about 65% of the population. Good crop development depends on the needed level of soil water reserve provided by precipitation. Perturbations of the hydrological cycle in response to climate change may involve perturbations of the frequency and intensity of precipitation and then directly affect the availability and quality of freshwater (Pal and Al-Tabbaa 2011). Should there be severe or recurrent droughts, major environmental and economic damage would result, with negative impacts such as soil degradation, decrease in agricultural production, and less hydroelectric energy production. Severe droughts were recorded in the Sahel region during the 1970s and 1980s and in many countries of the Horn of Africa, where they were more frequent, and the situation has persisted up to the first decade of the twenty-first century (Kandji et al. 2006). The sad consequences are usually widespread starvation and death (Druyan 2011; UNEP 2002). Therefore, there is the need to better understand droughts and to study their temporal and spatial variabilities under the current and future perturbed climate so as to guide vulnerability and adaptation assessments and measures.

Droughts are apparent after a long period with a shortage of precipitation or without any precipitation (Vicente-Serrano et al. 2010). Many definitions and related mathematical tools for their quantification have been developed. Among the most widely used are the traditional Palmer drought severity index (PDSI; Palmer 1965) and the standardized precipitation index (SPI; McKee et al. 1993). The PDSI is a soil moisture algorithm that includes terms for water storage and evapotranspiration, whereas the SPI is a probability index that is based solely on precipitation. It was formulated by McKee et al. (1993) to give a better representation of abnormal wetness and dryness than does the PDSI. The SPI can be defined as the number of standard deviations by which a normally distributed

Corresponding author address: G. M. Guenang, Laboratory for Environmental Modelling and Atmospheric Physics, Dept. of Physics, University of Yaoundé 1, P.O. Box 812 Yaoundé, Cameroon.
E-mail: merlin.guenang@yahoo.fr

DOI: 10.1175/JAMC-D-14-0032.1

random variable deviates from its long-term mean. For precipitation, it is mostly used to quantify deficits (droughts) on many time scales. The SPI has many advantages over the PDSI (Hayes et al. 1999). It depends only on precipitation and can be used for both dry and rainy seasons. It can describe drought conditions that are important for a range of meteorological, agricultural, and hydrological applications. Studies have shown that the SPI is suitable for quantifying most types of drought events (Mishra and Desai 2005; Szalai and Szinell 2000). Calculated at various time scales (from 1 to n months), SPI values can be efficient for the description of streamflow (on 2–6-month time scales), agricultural drought (on 2–3-month time scales), and groundwater level (on 5–24-month time scales) (Lloyd-Hughes and Saunders 2002). Some workers have stated that, because it depends only on precipitation, the SPI is not affected by topography (Hayes et al. 1999; Lloyd-Hughes and Saunders 2002; Lana et al. 2001).

In recent decades, many studies using the SPI were undertaken. Using the SPI extended to the Northern Hemisphere, Bordi and Sutera (2001) showed that there are some interesting spatially remote teleconnections that link the tropical Pacific Ocean with the European area. Lloyd-Hughes and Saunders (2002) found that trends in SPI values indicate significant change in the proportion of Europe experiencing extreme and/or moderate drought conditions during the twentieth century. SPI analysis satisfactorily explained the recurrent floods in the past 25 years that have affected the southern Cordoba Province in Argentina (Seiler et al. 2002). Livada and Assimakopoulos (2007) used the SPI to detect spatial and temporal drought events over Greece and found mild to moderate drought reduction from north to south and from west to east on 3- and 6-month time scales over the 51-yr time period of the study. In that study, the frequency of occurrence of severe and extreme drought conditions was very low on the 12-month time scale. The SPI was also used in China to study drought/wetness episodes in the Pearl River basin, and the results were helpful for basin-scale water resource management under a changing climate (Zhang et al. 2009). Thus, the SPI is widely used (Vicente-Serrano 2006). Its main weaknesses are dependence on the normalization procedure (the probability density function used) (Quiring 2009) and poor definition in arid regions that experience many months with zero precipitation (Wu et al. 2007). For Africa in particular, there are only a few studies on drought monitoring by use of climate indices. Ntale and Gan (2003) used the SPI as a drought indicator in the East African region and compared its performance with the PDSI and the Bhalme–Mooley index. The identification of droughts in Zimbabwe by Manatsa et al. (2008) on the basis of SPI estimation from the regionally averaged rainfall for 1900–2000 revealed that the most extreme droughts of the twentieth century were recorded in 1991 and 1992. Yuan et al. (2013) more recently used dynamical models to obtain probabilistic seasonal drought forecasts in Africa. This low number of past studies is one of the motivations of the current study.

In many studies that use the SPI, the gamma distribution is found to fit the precipitation data very well (Lloyd-Hughes and Saunders 2002) and to provide the best model for describing monthly precipitation. In the study over Cameroon that is presented here, we will go through the full process of distribution selection by fitting many distribution functions to the data and will use an appropriate statistical test to select the best fit for calculating the SPI at time scales of 3, 6, 12, 18, and 24 months. This selection is carried out at every station and at grid points for recorded and gridded University of East Anglia (United Kingdom) Climatic Research Unit (CRU) data. The ultimate purpose is to provide useful information for monitoring and managing water resources in agriculture, domestic/industrial uses, and hydroelectric energy production. The study can also help to understand better the historical variability of drought events and their relative intensity. We will also evaluate the usefulness of a spatialized dataset (CRU gridded precipitation) in reproducing station results and thus guide their use in areas without measuring stations. This paper is organized as follows: In the next section, the study area and data used are described. Section 3 gives details of SPI calculation and statistical distribution functions used to fit the data. Section 3f describes the method. Results are presented in section 4, and the paper ends with discussion and concluding remarks in section 5.

2. Study domain and data used

a. Study domain

Cameroon is located in equatorial central Africa between 1° and 13°N and between 7° and 18°E. The southern part of the country is bordered in the west by the Atlantic Ocean and is covered by dense rain forest. The northern part has a dry to arid Sahelian-type climate, depending on latitude. The main economic activity in the area is agriculture, generally at the subsistence level. Cassava, corn, yam, sweet potato, and millet are grown for food. Cacao, coffee, banana, rubber, palm oil, and cotton are the main cash crops raised by farmers. Logging is another important resource in Cameroon, with heavy timber exportation. These activities are mostly rainfed, and the use of irrigation is very marginal.

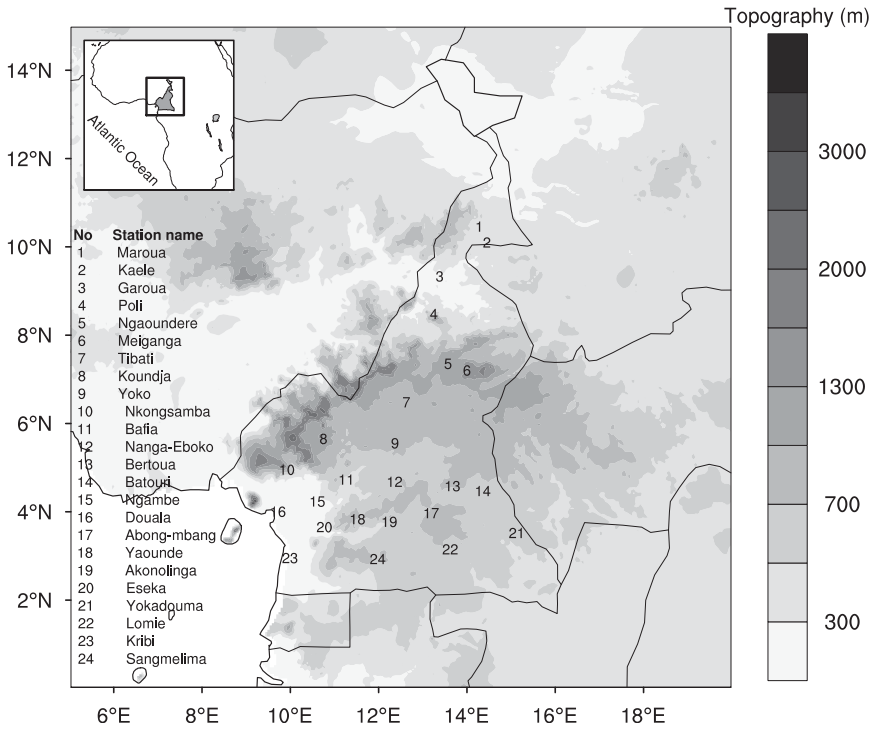

FIG. 1. Study area with the geographical locations of rainfall stations (indicated by numbers). The topography is shaded.

b. Data used

Monthly precipitation data used in this study derive from daily precipitation of 24 measuring stations in Cameroon as provided by the Cameroon Meteorological Service. The geographical positions of these stations and the topography of the domain are shown in Fig. 1. The precipitation record extends from 1951 to 2005 (55 yr). Part of this dataset was used by Penlap et al. (2004) and more recently by Guenang and Mkankam Kamga (2012). Overall, approximately 8.6% of the values are missing. One station (Nkongsamba) has no missing values, nine (Douala, Meiganga, Kribi, Ngaoundéré, Koundja, Bertoua, Poli, Yaoundé, and Garoua) have fewer than 4% of values that are missing, and seven (Abong-Mbang, Yokadouma, Sangmélima, Batouri, Yoko, Ngambe, and Lomié) are missing between 4% and 11% of their values. Gridded precipitation data from the CRU were also used to calculate the SPI on the study domain. Since many stations of the domain were used in the construction of the CRU gridded precipitation, these two datasets are not independent (New et al. 1999, 2000). Version 3.0 of the CRU precipitation data (Harris et al. 2014) is available at a monthly time scale on 0.5° × 0.5° longitude/latitude spatial grids. These data are unrestricted and at the time of writing were available for download from the Internet (http://badc.nerc.ac.uk/data/cru/).

3. Method

a. Calculation procedure for the SPI

The method used for SPI computation was developed by McKee et al. (1993) and Edwards and McKee (1997) to study relative departures of precipitation from normality. It has been widely applied in many studies (Vicente-Serrano 2006; Vicente-Serrano et al. 2010). It uses monthly precipitation aggregates at various time scales (1, 3, 6, 12, 18, and 24 months, etc.). As an illustration of the procedure, for a 3-month time scale, the precipitation accumulation from month $j - 2$ to month j is summed and attributed to month j. At this time scale, the first two months of the data time series are missing. Next follows the normalization procedure, in which an appropriate probability density function is first fitted to the long-term time series of aggregated precipitation. Then the fitted function is used to calculate the cumulative distribution of the data points, which are finally transformed into standardized normal variates. This procedure is repeated for all needed time scales. Because the processes that generate rainfall in our study domain vary in time and in space, many distributions may be needed to cover all time scales and stations. The maximum-likelihood (ML) estimation method was used to fit four probability distribution functions (i.e., gamma,

TABLE 1. Drought classification by SPI value and USDM drought definition.

Drought classification by SPI value		USDM drought definition (Svoboda et al. 2002)		
SPI value	Class	Category	Description	Percentile
2.00 or more	Extremely wet	—	—	—
1.50–1.99	Severely wet	—	—	—
1.00–1.49	Moderately wet	—	—	—
0–0.99	Mildly wet	—	—	—
From 0 to −0.99	Mild drought	D0	Abnormally dry	21%–30%
From −1.00 to −1.49	Moderate drought	D1	Moderate drought	11%–20%
From −1.50 to −1.99	Severe drought	D2	Severe drought	6%–10%
−2 or less	Extreme drought	D3	Extreme drought	3%–5%
—	—	D4	Exceptional drought	<2%

exponential, Weibull, and lognormal) to each time series. The one with the lowest value of the Anderson–Darling goodness-of-fit test statistic (Anderson and Darling 1952, 1954) was retained as representing the underlying distribution of the data.

b. SPI interpretation and operational drought definition

The SPI, often called the z score, is the number of standard deviations from the mean at which an event occurs. Thus, the 3-month SPI value provides a comparison of accumulated precipitation over that specific 3-month period with the mean precipitation total for the same annual period as calculated over the full study period. This applies to any n-month SPI value, where n, the number of months of accumulation, is the time scale. For precipitation, high positive values correspond to wet sequences and high negative values correspond to drought periods. For drought evaluation (negative SPI), short time scales on the order of 3 months may be important for agricultural applications, whereas long time scales of up to many years are of more interest in water-supply management (Guttman 1998). Many classifications of dryness and wetness events as based on the SPI have been proposed in the literature. An example is shown in Table 1 (Lloyd-Hughes and Saunders 2002). To use indices such as the SPI for operational monitoring, it is necessary to define drought threshold levels for preventive or corrective actions. Goodrich and Ellis (2006) proposed using preselected percentiles of the index to determine thresholds, as based on fitted empirical distributions. Quiring (2009) improved on the technique by using percentile values from distributions fitted to the data to define more-objective drought levels. Table 1 (columns 1 and 2) also shows the five-category drought definition from the U.S. Drought Monitor (USDM), with their description and corresponding percentiles (Svoboda et al. 2002). Here, we use the Quiring technique (Quiring 2009) and the percentile intervals of this table to determine drought in our domain.

c. The ML estimation method

The ML estimation method maximizes the probability of the observed data under a selected distribution. Applied to a dataset, it provides values of the distribution parameters that maximize the likelihood function (Wilks 2006).

Let x_i $(i = 1, \ldots, n)$ be a sample of n independent and identically distributed observations coming from a population with an underlying probability density function $f(.\,|\,\theta_0)$, where θ_0 is the unknown distribution parameter. It is desirable to find an estimator $\hat{\theta}$ that would be as close to the true value θ_0 as possible.

The joint density function for an independent and identically distributed sample is defined as

$$f(x_1, x_2, \ldots, x_n\,|\,\theta) = f(x_1\,|\,\theta) \times f(x_2\,|\,\theta) \times \cdots \times f(x_n\,|\,\theta). \tag{1}$$

If x_i are fixed parameters of this function and θ is the function's variable that is allowed to vary freely, then the function will be called the likelihood function:

$$\mathcal{L}(\theta\,|\,x_1, \ldots, x_n) = f(x_1, x_2, \ldots, x_n\,|\,\theta) = \prod_{i=1}^{n} f(x_i\,|\,\theta). \tag{2}$$

In practice, the log-likelihood is more convenient. It is the logarithm of the likelihood function so that

$$\ln\mathcal{L}(\theta\,|\,x_1, \ldots, x_n) = \sum_{i=1}^{n} \ln f(x_i\,|\,\theta). \tag{3}$$

The average log-likelihood can also be used:

$$\hat{\ell} = n^{-1} \ln\mathcal{L}. \tag{4}$$

The term $\hat{\ell}$ estimates the expected log-likelihood of a single observation in the model. The ML method estimates θ_0 by finding a value of θ that maximizes $\hat{\ell}(\theta\,|\,x)$.

d. Distributions used to fit the data

1) THE GAMMA DISTRIBUTION FUNCTION

The probability density function of the gamma distribution is defined as

$$g(x) = \frac{1}{\beta^{\alpha}\Gamma(\alpha)} x^{\alpha-1} e^{-x/\beta} \quad \text{for} \quad x > 0, \tag{5}$$

where $\alpha > 0$ is a shape parameter, $\beta > 0$ is a scale parameter, $x > 0$ is the amount of precipitation, and $\Gamma(\alpha)$ is the gamma function. More detailed descriptions of the gamma distribution can be found in Lloyd-Hughes and Saunders (2002) and Guttman (1999).

To fit the distribution parameters, α and β are estimated from the sample data. Using the approximation for ML defined by Thom (1958), they can be estimated as

$$\hat{\alpha} = \frac{1}{4A}\left(1 + \sqrt{1 + \frac{4A}{3}}\right) \quad \text{and} \tag{6}$$

$$\hat{\beta} = \overline{x}/\hat{\alpha}, \tag{7}$$

where $\overline{x}$ is mean precipitation and A is given by

$$A = \ln(\overline{x}) - n^{-1}\sum \ln(x). \tag{8}$$

Under some conditions, α and β can be better estimated by using an iterative procedure as suggested by Wilks (1995).

For a given month and time scale, the cumulative probability $G(x)$ of an observed amount of precipitation is given by

$$G(x) = \frac{1}{\hat{\beta}^{\hat{\alpha}}\Gamma(\hat{\alpha})} \int_0^x x^{\hat{\alpha}} e^{-x/\hat{\beta}}\, dx. \tag{9}$$

Letting $t = x/\hat{\beta}$, we reduce the expression to the following function, called the incomplete gamma function:

$$G(x) = \frac{1}{\Gamma(\hat{\alpha})} \int_0^x t^{\hat{\alpha}-1} e^{-1}\, dt. \tag{10}$$

The gamma distribution is not defined for $x = 0$, and, the probability of zero precipitation $q = P(x = 0)$ being positive, the cumulative probability becomes

$$H(x) = q + (1 - q)G(x). \tag{11}$$

2) THE EXPONENTIAL DISTRIBUTION FUNCTION

The general formula for the probability density function of the exponential distribution is stated as (Ahmad and Bhat 2010)

$$f(x) = \frac{1}{\beta} e^{-(x-\mu)/\beta} \quad \text{for} \quad x \geq \mu \quad \text{and} \quad \beta > 0, \tag{12}$$

where μ is the location parameter and β is the scale parameter. The scale parameter is often referred to as $\lambda = 1/\beta$ and is called the constant failure rate. The terms μ and β can be estimated from an independent and identically distributed sample $x = (x_1, \ldots, x_n)$ drawn from the variable using the ML estimation method (Ross 2009):

$$\hat{\lambda} = 1/\overline{x}, \tag{13}$$

where

$$\overline{x} = n^{-1}\sum_{i=1}^{n} x_i.$$

3) THE LOGNORMAL DISTRIBUTION FUNCTION

In probability theory, a positive random variable x follows the lognormal (μ, σ^2) distribution if the logarithm of the random variable is normally distributed. The probability density function of a lognormal distribution is defined as (Bartosova 2006; Bilkova 2012)

$$f(x;\mu,\sigma) = \frac{1}{x\sigma\sqrt{2\pi}} \exp\left[-\frac{(\ln x - \mu)^2}{2\sigma^2}\right], \quad x > 0, \tag{14}$$

where $x > 0$, $-\infty < \mu < +\infty$, and $\sigma > 0$. The term μ is the scale parameter that stretches or shrinks the distribution, and σ is the shape parameter that affects the shape of the distribution. They can be determined by the ML estimators:

$$\hat{\mu} = n^{-1}\sum_{k} \ln x_k \quad \text{and} \tag{15}$$

$$\hat{\sigma}^2 = n^{-1}\sum_{k} (\ln x_k - \hat{\mu})^2. \tag{16}$$

4) THE WEIBULL DISTRIBUTION FUNCTION

The probability density function of a Weibull random positive variable x is (Wu 2002; Panahi and Asadi 2011)

$$f(x;\alpha,\beta) = \alpha\beta x^{\alpha-1} e^{-\beta x^{\alpha}}, \tag{17}$$

where α and β are the shape and scale parameters, respectively. Its complementary cumulative distribution function is a stretched exponential function. The Weibull distribution is related to a number of other probability distributions; in particular, it interpolates between the exponential distribution ($k = 1$) and the Rayleigh distribution ($k = 2$). There are no closed-form expressions of the parameters $\hat{\alpha}$ and $\hat{\beta}$, and therefore

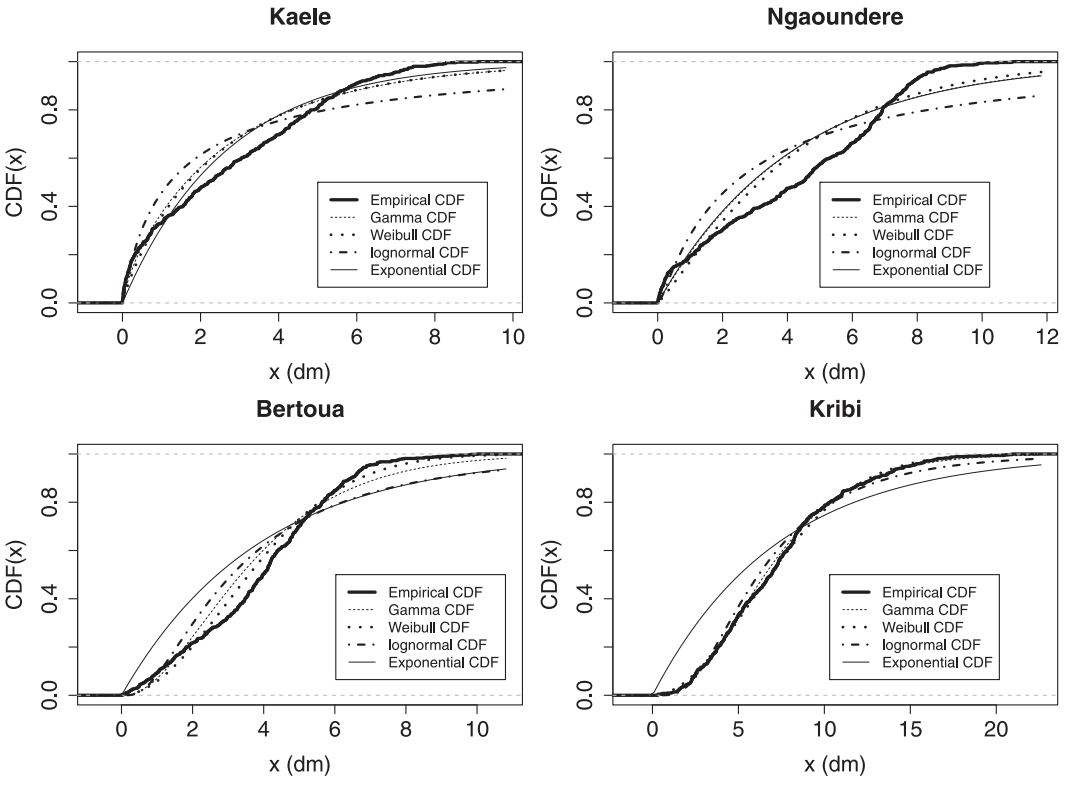

FIG. 2. Cumulative distribution functions for 3-month aggregated precipitation showing the empirical cumulative distribution function and gamma, Weibull, lognormal, and exponential distributions fitted to the data.

they are estimated by maximizing the log-likelihood expression of Eq. (3) (Panahi and Asadi 2011).

e. Statistical tests used

1) THE ANDERSON AND DARLING STATISTICAL TEST

The Anderson–Darling statistic A^2 measures how well a given data sample X_i ($i = 1, \ldots, n$) follows a particular distribution function F. The statistic is defined as (Anderson and Darling 1952, 1954)

$$A^2 = -n - n^{-1} \sum_{i=1}^{n} (2i-1)\{\ln[F(X_i)] + \ln[1 - F(X_{n+1-i})]\}. \quad (18)$$

For a given dataset and distribution function, the better that the distribution fits the data, the smaller this statistic will be. The hypothesis regarding the distributional form is rejected at the chosen significance level α if the test statistic A^2 is greater than the critical value obtained from a table.

2) THE KOLMOGOROV–SMIRNOV GOODNESS OF FIT

The Kolmogorov–Smirnov (K–S) test is a nonparametric test that can be used to compare a sample with a reference probability distribution or to compare two samples. It quantifies a distance between the empirical distribution function of the sample and the cumulative distribution function of the reference distribution or between the empirical distribution functions of two samples.

For a given cumulative distribution function $F(x)$, the K–S statistic is defined as (Stephens 1970)

$$D_n = \max_x |F_n(x) - F(x)|, \quad (19)$$

where n is the number of observations in the population x, $F_n(x)$ is the empirical cumulative distribution function, and $F(x)$ is the theoretical cumulative distribution function. The K–S test can be modified to serve as a goodness-of-fit test. In the special case of testing for normality of the distribution, samples are standardized and are compared with a standard normal distribution.

f. Study steps

SPI time series were calculated for all stations and for the CRU grid point nearest to each station. This procedure is expected to lead to normally distributed SPI, but this is not always the case. Since the Quiring technique (Quiring 2009) requires fitting a statistical distribution to the SPI, five distributions including the normal were tested, and then the K–S goodness-of-fit test

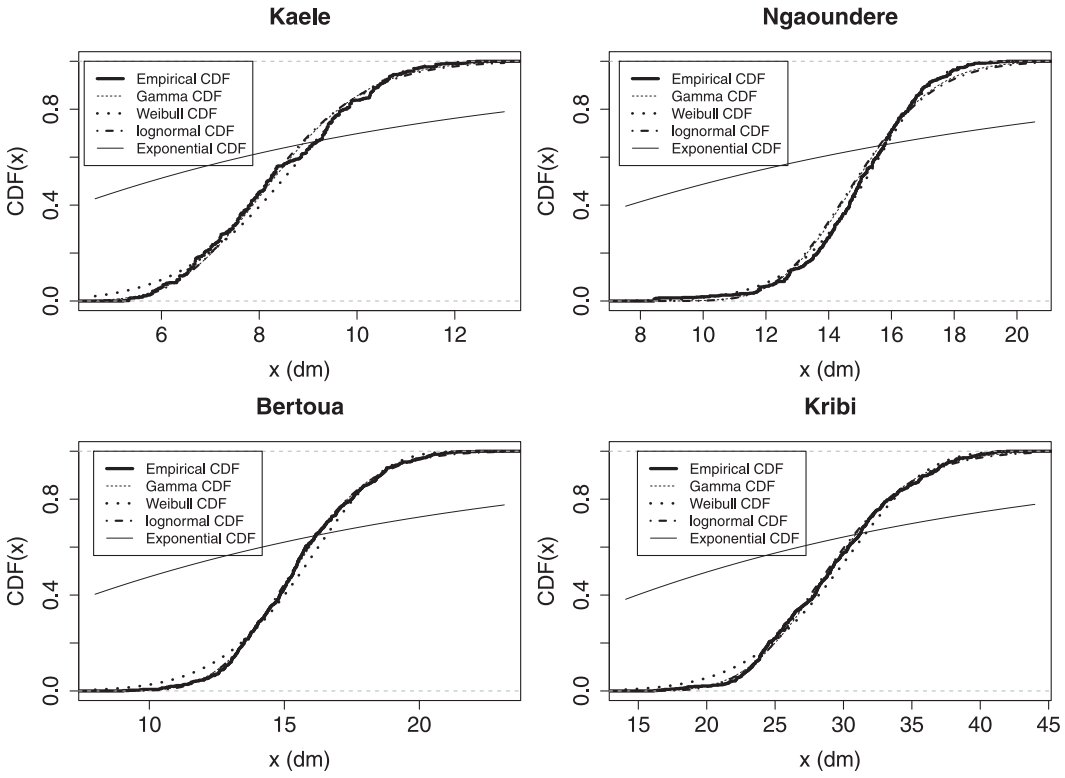

FIG. 3. As in Fig. 2, but for 12-month aggregated precipitation.

statistic was used at the 5% significant level. In almost all instances, the Weibull and normal distributions had the lowest (and also close) K–S test statistics. Operational drought thresholds were therefore calculated on the basis of the normal distribution and on percentiles defined by Svoboda et al. (2002) (Table 1). Analyses of the results focused on four stations (Kaélé, Ngaoundéré, Bertoua, and Kribi), one in each of four different known climatic zones of the study domain. These zones are characterized by similar rain and physical atmospheric processes. Each station has the least amount of missing data in its zone. The station of Kaélé is located north of the domain in the Sahelian zone, Ngaoundéré is in the Adamawa Plateau in the middle part of the domain, Bertoua is in the eastern part in dense forest, and Kribi is in the southwestern part closest to the Atlantic Ocean (Fig. 1).

4. Results

a. Suitable distribution functions for precipitation data

1) DISTRIBUTION FUNCTIONS FOR STATION PRECIPITATION

Four statistical distribution functions (gamma, exponential, Weibull, and lognormal) were fitted to station precipitation data aggregated at various time scales. Figures 2 and 3 show results of the cumulative distribution function for empirical precipitation and for each of the trial distribution functions. Figures are shown for four stations (Kaélé, Ngaoundéré, Bertoua, and Kribi) at 3- and 12-month time scales. The choice of the suitable distribution function describing precipitation data in each case was based on the minimum value of the Anderson–Darling statistic, as illustrated in Table 2 for 3- and 12-month time scales. The exponential function shows worse results as the number of months in the time scale increases. Table 3 recapitulates these results, extended to other stations and to various time scales. The functions are represented by letters [i.e., gamma (g), Weibull (w), exponential (e), and logormal (ln)]. It appears that, for time scales equal to 6 months and less, the distribution of station precipitation shows a bias for the Weibull function to be suitable for the highest number of stations (21 for both 1- and 3-month time scales and 16 for 6-month time scale) of the 24 studied stations. The gamma function outperformed the others in very few cases. One exceptional case of exponential and lognormal being best is observed for 1- and 6-month time scales, respectively. Above the 6-month time scale, the number of station precipitation distributions being best fitted by the

TABLE 2. Anderson–Darling test statistics calculated at 95% confidence level for the four distributions and two time scales; the distribution function key is given in the text. The smallest value at each station is in boldface.

No.	Station	For 3-month time scale				For 12-month time scale			
		g	w	e	ln	g	w	e	ln
1	Maroua	**8.12**	9.24	11.16	18.72	1.48	9.45	184	**1.13**
2	Kaélé	**8.91**	10.20	13.36	21.50	**2.03**	3.84	171	2.22
3	Garoua	13.10	**12.19**	14.08	25.52	1.58	9.31	195.8	**1.04**
4	Poli	18.88	**18.35**	18.58	35.65	**1.08**	3.46	207.7	1.59
5	Ngaoundéré	24.21	**23.20**	24.43	41.22	4.84	**1.36**	218	6.76
6	Meiganga	17.36	**16.08**	18.51	34.30	1.03	6.96	223.9	**0.91**
7	Tibati	19.37	**17.15**	21.09	37.43	**0.72**	3.88	199.8	1.24
8	Koundja	16.22	**12.87**	22.70	35.21	**0.90**	4.35	223.8	1.12
9	Yoko	16.40	**13.01**	23.83	30.83	1.08	5.10	167.9	**0.91**
10	Nkongsamba	8.15	**7.099**	14.15	19.84	**1.20**	3.60	229	1.89
11	Bafia	20.55	**13.62**	45.14	36.81	**1.81**	5.99	200	2.24
12	Nanga-Eboko	12.36	**6.65**	43.15	26.78	4.97	**0.72**	179	6.91
13	Bertoua	15.19	**7.65**	58.47	30.30	**0.47**	5.41	210.8	0.53
14	Batouri	11.48	**6.02**	49.79	21.08	**1.21**	2.68	165.9	1.57
15	Ngambe	5.50	**4.18**	12.81	14.85	**2.35**	3.09	172	2.59
16	Douala	4.62	**4.32**	14.37	10.63	**3.58**	4.15	213	3.9
17	Abong-Mbang	10.99	**5.02**	54.07	22.15	**1.46**	5.78	183	2.03
18	Yaoundé	11.41	**5.69**	58.96	22.46	**0.51**	4.24	217.7	0.96
19	Akonolinga	10.98	**5.58**	56.85	21.06	2.30	**1.43**	186	3.12
20	Eséka	11.61	**5.37**	58.21	22.31	0.81	7.75	183.7	**0.48**
21	Yokadouma	11.51	**5.61**	61.34	20.96	**2.50**	5.82	187	3.67
22	Lomié	8.04	**3.12**	58.36	15.48	**1.03**	8.48	161.7	1.05
23	Kribi	**0.70**	0.84	61.56	4.77	**0.94**	4.24	200	1.15
24	Sangmélima	6.25	**1.63**	70.84	13.34	0.86	10.6	184	**0.56**

Weibull function decreases, falling to three and seven (three stations for 12 and 18 months, and seven for 24 months) to the benefit of the gamma function, which is suitable for up to 18 stations at the 18-month time scale. The number of station precipitation distributions following the lognormal function also increases with the number of months in the time scale, reaching 8 stations of 24 by 24 months.

Figure 4 shows the spatial pattern of the suitable distribution functions over the domain of study for 3- (Fig. 4a), 6-,and 12- (Fig. 4b), and 18- and 24-month (Fig. 4c) time scales. For not more than a 3-month time scale (illustration for 3 months in Fig. 4a), the gamma distribution function is suitable north of the domain (Sahelian region), particularly above 10°N, while below that the Weibull function is the best fit, except for a single case at the boundary of the Atlantic Ocean that shows a bias to the gamma function. The Weibull function remains the most suitable at the 6-month time scale between 4° and 10°N, which represents the transition zone between the Sahelian and equatorial forest zones. Stations of the equatorial forest zone, covering the southern plateau (below 4°N), mostly show a bias for the gamma distribution. At a 12-month time scale and beyond, there is a mixture of gamma, lognormal, and Weibull distributions in different zones, leading to no apparent spatial organized pattern (Figs. 4b,c). The pattern for the 18-month time scale looks more like that of 6 months but with the gamma function in place of the Weibull function. An almost equal number of gamma [(9)], lognormal [(8)], and Weibull [(7)] functions fit the 24-month time scale, with no particular spatial organization. These apparent inconsistencies are due to the fact that in most cases more than one distribution was adequate and the Anderson–Darling statistics may not have been significantly different. Between 18- and 24-month time scales, the number of station data showing a bias for the lognormal function increases up to 8 in the southwestern part of the domain (right of the Atlantic Ocean).

2) DISTRIBUTION FUNCTIONS FOR CRU PRECIPITATION

Distribution functions were also fitted to precipitation time series of the CRU grid point that is nearest to each station of the study domain. The results are in Table 3, where the last column indicates the number of cases of the six time scales analyzed for which the same distribution functions fitted both station and CRU data. The highest number of agreements across time scales between the two datasets is obtained in the southeastern part of the domain (Batouri and Yokadouma stations).

TABLE 3. Selected distribution functions for station precipitation data at various time scales. In the last column is the number of times the same distribution fits both the station and the CRU data.

No.	Station	Best distribution for n-month time scale						No. of CRU agreement of six possible
		$n = 1$	$n = 3$	$n = 6$	$n = 12$	$n = 18$	$n = 24$	
1	Maroua	g	g	g	ln	w	g	3
2	Kaélé	g	g	w	g	g	ln	5
3	Garoua	w	w	w	ln	w	g	4
4	Poli	w	w	w	g	g	w	4
5	Ngaoundéré	w	w	w	w	g	w	3
6	Meiganga	w	w	w	ln	g	ln	1
7	Tibati	w	w	w	g	g	w	5
8	Koundja	w	w	w	g	g	g	3
9	Yoko	w	w	w	ln	g	ln	3
10	Nkongsamba	w	w	w	g	g	g	4
11	Bafia	w	w	w	g	g	g	5
12	Nanga-Eboko	w	w	w	w	w	w	3
13	Bertoua	w	w	w	g	g	w	5
14	Batouri	w	w	w	g	g	ln	6
15	Ngambe	e	w	w	g	g	w	4
16	Douala	w	w	w	g	g	ln	5
17	Abong-Mbang	w	w	g	g	g	w	4
18	Yaoundé	w	w	g	g	g	g	2
19	Akonolinga	w	w	g	w	g	g	4
20	Eséka	w	w	g	ln	ln	ln	2
21	Yokadouma	w	w	w	g	g	g	6
22	Lomié	w	w	g	g	g	g	5
23	Kribi	w	g	ln	g	ln	ln	3
24	Sangmélima	w	w	g	ln	ln	ln	3

In three instances, there was agreement on fewer than three time scales, that is, Yaoundé and Eseka in the south and Ngaoundéré on the Adamawa Plateau. Overall, stations and CRU gridded precipitation are mostly fitted by the same functions.

b. Analysis of the SPI for different time scales

1) OPERATIONAL DROUGHT THRESHOLDS

The operational drought thresholds as described in section 3 were calculated for all stations for the five

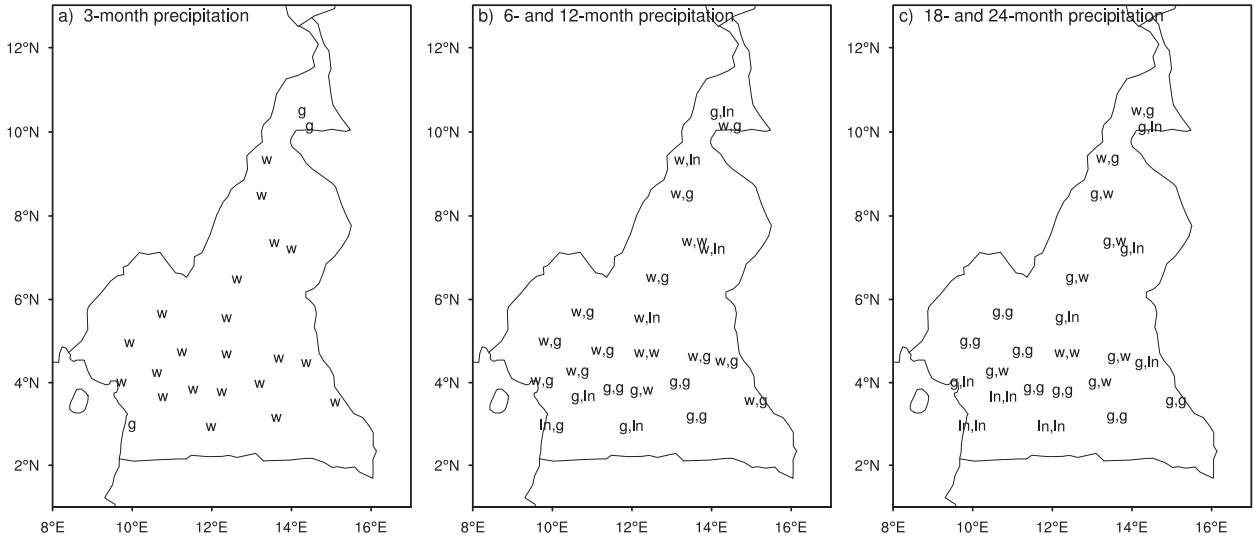

FIG. 4. Spatial pattern of chosen distribution function for (a) 3-month, (b) 6- and 12-month, and (c) 18- and 24-month precipitation; the distribution key is given in the text. In (b) and (c), the first letter refers to the first time scale and the second letter to the second time scale in the figure.

TABLE 4. Operational drought thresholds for various drought categories and for all stations, calculated using 3- and 12-month SPI.

No.	Station name	Drought category for 3 month					Drought category for 12 month				
		D4	D3	D2	D1	D0	D4	D3	D2	D1	D0
1	Maroua	−2.03	−1.74	−1.5	−1.02	−0.59	−1.64	−1.47	−1.32	−0.94	−0.71
2	Kaélé	−2.08	−1.86	−1.47	−1.04	−0.62	−1.64	−1.47	−1.32	−0.94	−0.71
3	Garoua	−2.25	−1.92	−1.49	−1.09	−0.51	−2.28	−1.61	−1.19	−0.74	−0.48
4	Poli	−2.49	−2.21	−1.58	−0.91	−0.55	−1.64	−1.47	−1.32	−0.94	−0.71
5	Ngaoundéré	−2.55	−2.05	−1.69	−0.93	−0.49	−2.05	−1.63	−1.2	−0.73	−0.47
6	Meiganga	−2.35	−1.9	−1.56	−0.99	−0.54	−1.64	−1.47	−1.32	−0.94	−0.71
7	Tibati	−2.66	−1.99	−1.54	−0.9	−0.47	−1.64	−1.47	−1.32	−0.94	−0.71
8	Koundja	−2.55	−1.83	−1.49	−0.9	−0.45	−1.57	−1.4	−1.24	−0.83	−0.61
9	Yoko	−2.44	−1.91	−1.48	−0.91	−0.45	−1.64	−1.47	−1.32	−0.94	−0.71
10	Nkongsamba	−1.97	−1.64	−1.45	−1.01	−0.55	−1.79	−1.57	−1.17	−0.83	−0.51
11	Bafia	−2.36	−1.94	−1.44	−0.99	−0.32	−1.64	−1.47	−1.32	−0.94	−0.71
12	Nanga-Eboko	−2.27	−1.74	−1.38	−0.9	−0.45	−1.64	−1.47	−1.32	−0.94	−0.71
13	Bertoua	−2.31	−1.77	−1.42	−0.9	−0.41	−1.64	−1.47	−1.32	−0.94	−0.71
14	Batouri	−2.2	−1.74	−1.45	−0.88	−0.5	−1.64	−1.45	−1.28	−0.92	−0.6
15	Ngambe	−1.98	−1.67	−1.37	−1	−0.54	−1.75	−1.61	−1.29	−0.85	−0.59
16	Douala	−1.73	−1.5	−1.31	−0.97	−0.62	−1.76	−1.5	−1.19	−0.9	−0.63
17	Abong-Mbang	−2.18	−1.71	−1.38	−0.84	−0.48	−1.64	−1.47	−1.32	−0.94	−0.71
18	Yaoundé	−2.16	−1.74	−1.45	−0.88	−0.49	−1.64	−1.47	−1.32	−0.94	−0.71
19	Akonolinga	−2.13	−1.7	−1.4	−0.94	−0.47	−1.93	−1.7	−1.44	−0.88	−0.46
20	Eséka	−2.06	−1.78	−1.46	−0.81	−0.46	−2.09	−1.65	−1.32	−0.85	−0.54
21	Yokadouma	−1.97	−1.71	−1.41	−0.91	−0.46	−1.64	−1.47	−1.32	−0.94	−0.71
22	Lomié	−1.94	−1.62	−1.32	−0.9	−0.51	−1.64	−1.47	−1.32	−0.94	−0.71
23	Kribi	−1.82	−1.46	−1.27	−0.83	−0.55	−1.64	−1.47	−1.32	−0.94	−0.71
24	Sangmélima	−1.85	−1.6	−1.24	−0.85	−0.52	−2.05	−1.58	−1.32	−0.85	−0.47

USDM categories of Table 1 (columns 3–5) and for 3- and 12-month time scales. All the values are shown in Table 4. In considering the extreme-drought category D4 for the 3-month time scale, it is seen that there is a range from a maximum of −1.73 in the coastal city of Douala to a minimum of −2.66 in Tibati on the Adamawa Plateau. The spatial distribution of D4 thresholds is coherent, with values of lower than −2.40 on the high grounds of the Adamawa Plateau. Continental stations located between latitudes 2° and 7°N have thresholds between −2.10 and −2.40. In the southern part of the domain and in the coastal area in the southwest, values are higher than −2.0. Values for the three Sahelian stations of Kaélé, Maroua, and Garoua are respectively −2.08, −2.03, and −2.25. At this scale, extreme-drought category D3 follows the general pattern of D4. For the 12-month SPI, most of the stations have a D4 threshold of −1.64, with only three stations below −2.0. From the spatial analysis of category D4, there is no strong dependence on topography, although most stations have very similar thresholds (−1.64) at a 12-month time scale.

2) FREQUENCY OF DROUGHT EVENTS

Objective drought thresholds were also used to examine frequency in the SPI time series. In Fig. 5, appropriate D4-category threshold values are represented by dashed horizontal lines and exceedances corresponding to drought occurrences. For the 3-month SPI (left column in Fig. 5), each station had at least one event with a value that was lower than −3. For the first 25 yr of the study period the four stations differ markedly in D4-category drought frequency (10 in Kaélé, 6 in Kribi, only 2 in Ngaoundéré, and none in Bertoua), whereas in the second half of the period these episodes are more frequent (two stations had 13 events each, and the other two had 8 events each). For the 12-month SPI, all categories of drought events are frequent, especially from the mid-1960s. The dramatic drought episodes of the 1970s and 1980s are clearly visible, with each station recording at least one D4 event. Table 5 summarizes drought occurrences in all categories, with the number of events and the percentage with respect to the total number of time steps in the data. For the 3-month time scale, this percentage is 1%–2% for exceptional droughts and around 5% for extreme droughts. For the 12-month time scale, the percentage remains low for all categories, ranging from 1% for D4 to 5% for D0 events.

3) STATION VS CRU SPI

Figure 6 presents 3- and 12-month scale SPI time series from the CRU grid point that is nearest to each of the four observations stations of Fig. 5. This choice is

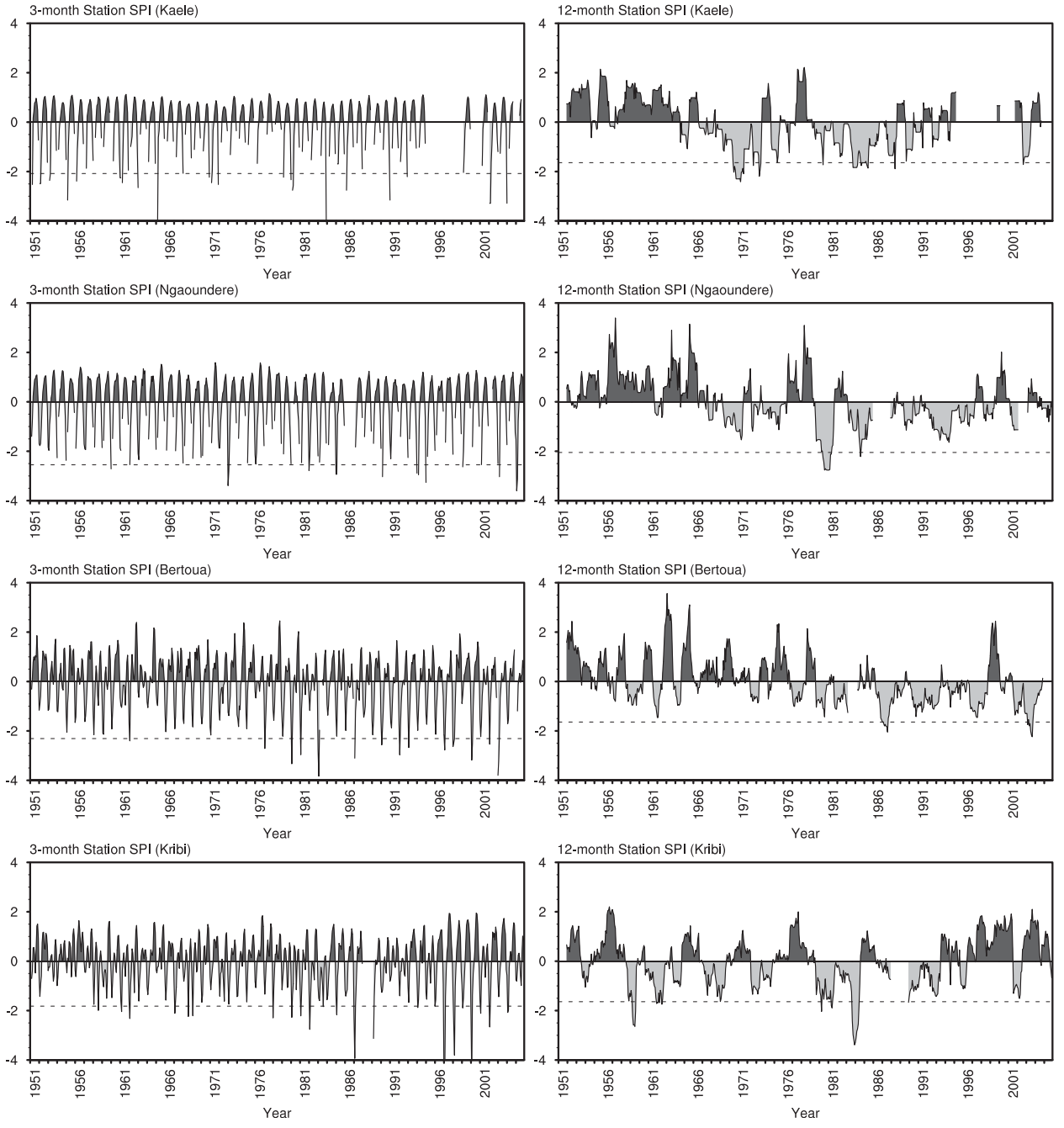

FIG. 5. Station SPI time series for the (left) 3- and (right) 12-month time scales. The horizontal dashed lines indicate operational drought thresholds for the exceptional-drought category (D4).

justified by the fact that the angular distance–weighted interpolation technique used to construct the CRU set gives more weight to the station that is nearest to the grid point, thus making it the best representative of the station. In this analysis, we compare these time series with those of the stations in Fig. 5 to access how well the gridded data reproduce drought characteristics obtained from station observations. For the 3-month-scale SPI, the two time series agree overall, with some discrepancies occurring at dates that differ from station to station: in Kaélé in the early 1950s, the 1970s, and the late 1980s; in Bertoua in the late 1990s; and in Kribi in the late 1990s, except for the drought of 1997. Most strong events that are present in the observations for at least three stations are reproduced in the gridded data, noticeably in 1962, 1967, 1983, 1987, 1997, and 2004. Of

TABLE 5. Number of drought events from 1951 to 2005 and for the five drought categories (D0, D1, D2, D3, and D4). Results in parentheses represent the percentage of realization of the event over the considered time period.

	No. of events for 3-month time scale				No. of events for 12-month time scale			
	Kaélé	Ngaoundéré	Bertoua	Kribi	Kaélé	Ngaoundéré	Bertoua	Kribi
D4	21 (4%)	11 (1%)	14 (2%)	23 (3%)	9 (1%)	2 (0%)	3 (0%)	8 (1%)
D3	26 (5%)	32 (5%)	32 (4%)	36 (5%)	10 (1%)	3 (0%)	2 (0%)	14 (2%)
D2	39 (8%)	53 (9%)	41 (6%)	45 (6%)	13 (2%)	6 (0%)	7 (1%)	20 (3%)
D1	59 (12%)	76 (13%)	53 (8%)	55 (8%)	16 (2%)	21 (3%)	24 (3%)	21 (3%)
D0	81 (17%)	90 (15%)	62 (9%)	66 (10%)	21 (3%)	32 (5%)	33 (5%)	27 (4%)

more concern are the results of Kaélé, where station data show high year-to-year variability of drought intensities, with six events with an SPI of less than −3, when CRU has an excessively large number of events of magnitude −2. At the same station, three strong events of the early 1950s are much weaker in the gridded data, whereas weak ones in the 1970s are amplified. For the other stations, CRU tends to show more severe droughts. Thus, for events with SPI values of less than −3, there are 12 against 5 in Bertoua, 11 against 7 in Ngaoundéré, but only 3 against 5 in Kribi. This reverse situation in Kribi is due to the underestimation of strong drought events between 1997 and 2000. For the 12-month-scale SPI, the main wet (1950s and late 1990s) and dry (1970s and 1980s) periods show up in both time series. Most drought events last many years, and CRU indicates more extreme values than do stations. The discrepancies noted at shorter time scales tend to be amplified at this and higher scales. Thus, in Kaélé, gridded data show a wet (against dry) episode in the mid-1960s and early 2000s and the reverse in 1994. This phase opposition between the two datasets is also found for the late 1960s in Ngaoundéré and the early 1970s and the 1990s in Bertoua. Amplification of disagreement between station and CRU data is better seen in Fig. 7, which shows multitime-scale SPI. A case in point is the 1996–2000 period in Kribi. On the 3-month scale (Fig. 6), the four years of severe droughts indicated by the station are underestimated by CRU. At the 12-month scale, the period is wet for both and more so for the station. This reversal is due to the strong wet peaks occurring in the same period at the station but not on the CRU grid, and that contributes to the longer-scale SPI. Overall, the CRU gridded data give a fair representation of drought events in the study area and can be used where no local station observations are available. The absence of missing data points is an additional advantage. It may, however, be of interest to evaluate the merits of using more than one grid point at a given site.

5. Discussion and conclusions

We tested four statistical distribution functions on precipitation data recorded at 24 stations in Cameroon for the time period extending from 1951 to 2005. The Anderson–Darling statistic was used to select the suitable distribution functions that were then used in the calculation of the standardized precipitation index. Results were compared with those obtained using CRU grid precipitation. Operational drought thresholds were also calculated for the five defined drought categories, and results were used to study the frequency of drought events at four stations that represent different climatic zones in the study domain. Multiscalar SPI for both station and CRU were finally compared to show the usefulness of gridded data.

It was found that the suitable distribution function underlying the data changes depended on station location and on the length of the time interval used for aggregation of precipitation. The Weibull and gamma are the functions that best fit precipitation in the area. In most studies on the SPI, the gamma distribution is chosen without any testing. The need for such an evaluation is even clearer for longer time scales where Weibull, gamma, and lognormal distributions are found, with no discernable pattern. We also found that objective drought thresholds are station specific for subannual scales but that the spatial distributions are coherent. Thus, regional values can be defined. For longer scales (above 12 months), most stations in the domain have the same threshold values. For most stations, drought magnitude and duration increased with time for both short and long time scales. This can be the consequence of a reduction in precipitation resulting from climate change as suggested by Vicente-Serrano et al. (2010). Such an increase in dryness probably affected crop development and river runoff negatively. The SPI, which is based only on precipitation, cannot explain the influence of temperature change on drought condition. Thus, Vicente-Serrano et al. (2010) suggested the calculation of a new index—the standardized precipitation evapotranspiration index—that is suited to detecting, monitoring, and exploring the consequences of global warming on drought conditions. Further studies taking into account this approach are necessary to better understand the climatological features of drought. With the increase in

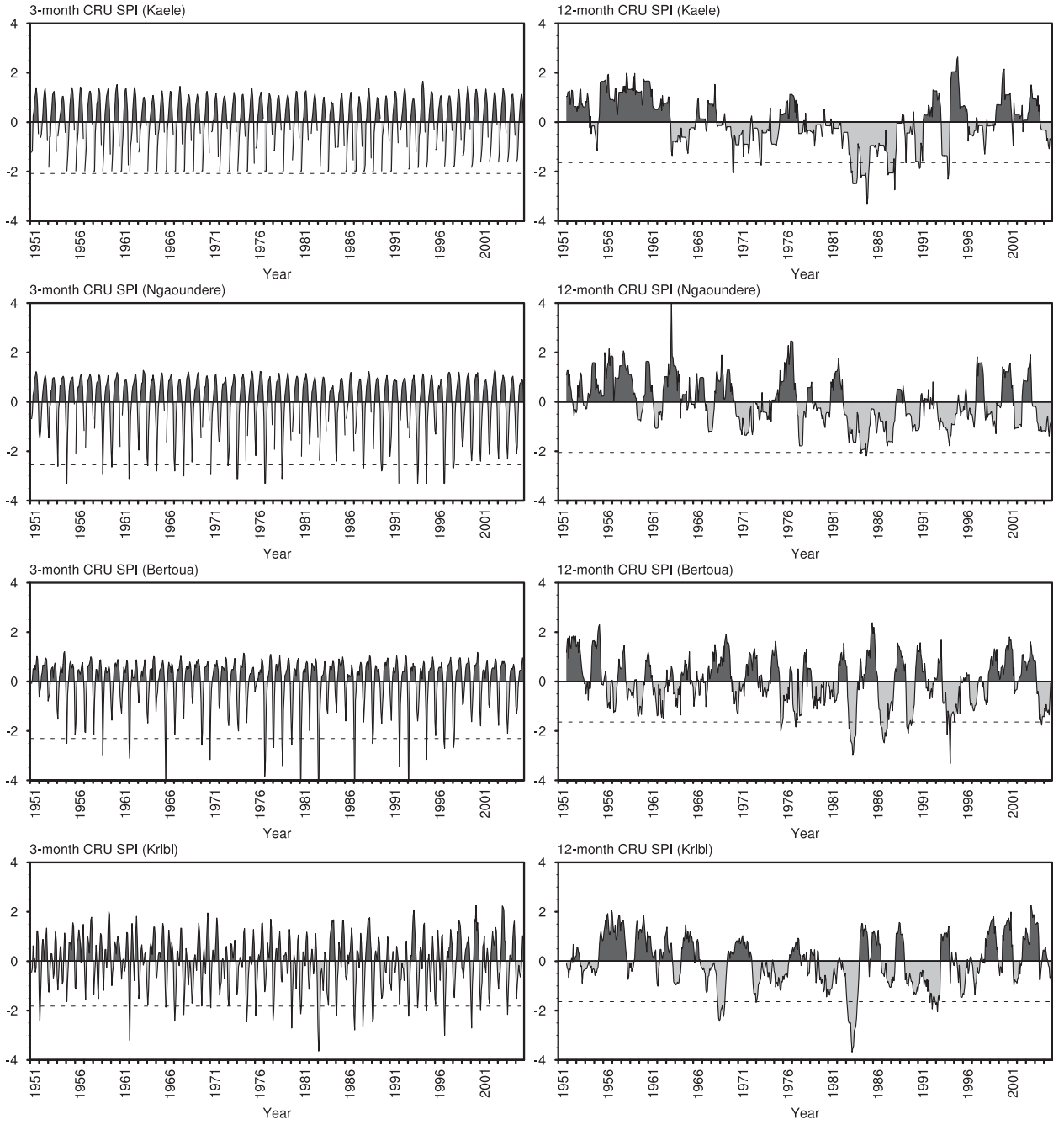

FIG. 6. The (left) 3- and (right) 12-month-scale SPI time series from the CRU grid point that is nearest to each of the four chosen stations.

global warming, an increase in drought magnitude, duration, and frequency is to be feared, and studies that include climate models and that are intended to guide adaptive measures also need to be done. CRU precipitation distribution functions and derived SPI corroborate the results of many stations, with some discrepancies at longer scales. Therefore, it is recommended that further investigations use CRU data for areas where observations are not possible or where they have high proportions of missing data.

Acknowledgments. The authors are grateful to the National Meteorological Service of Cameroon (DNMC) for providing station precipitation data. The CRU monthly precipitation data were produced by the Climatic Research Unit of the University of East Anglia.

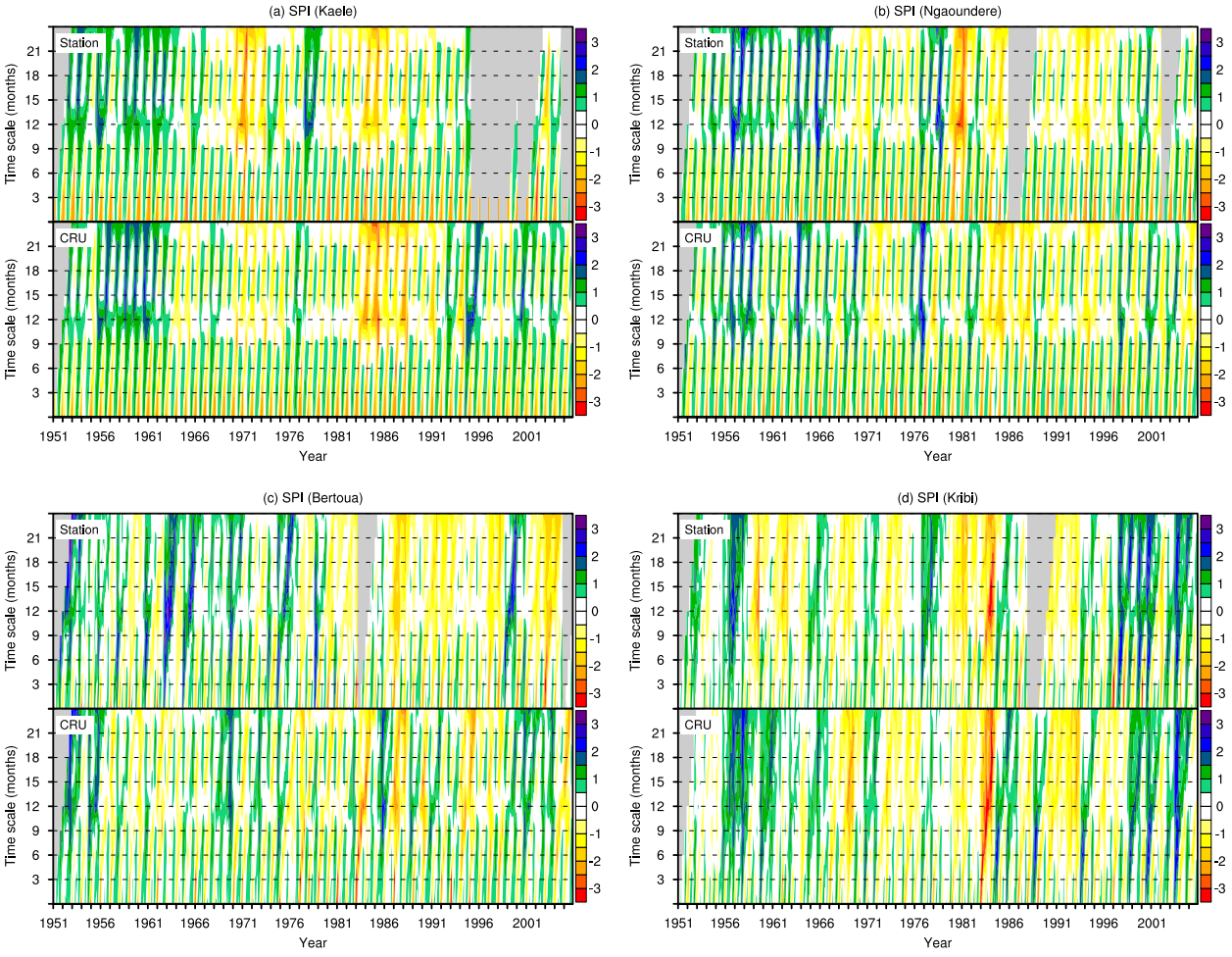

FIG. 7. Station and CRU SPI for four stations.

REFERENCES

Ahmad, S., and B. A. Bhat, 2010: Posterior estimates of two parameter exponential distribution using S-PLUS software. *J. Reliab. Stat. Stud.,* **3,** 27–34. [Available online at http://www.jrss.in/data/323.pdf.]

Anderson, T. W., and D. A. Darling, 1952: Asymptotic theory of certain goodness-of-fit criteria based on stochastic processes. *Ann. Math. Stat.,* **23,** 193–212, doi:10.1214/aoms/1177729437.

——, and ——, 1954: A test of goodness-of-fit. *J. Amer. Stat. Assoc.,* **49,** 765–769, doi:10.1080/01621459.1954.10501232.

Bartosova, J., 2006: Logarithmic-normal model of income distribution in the Czech Republic. *Austrian J. Stat.,* **35,** 215–222. [Available online at http://www.stat.tugraz.at/AJS/ausg062+3/062Bartosov.pdf.]

Bilkova, D., 2012: Lognormal distribution and using L-moment method for estimating its parameters. *Int. J. Math. Models Methods Appl. Sci.,* **6,** 30–44. [Available online at http://naun.org/main/NAUN/ijmmas/17-079.pdf.]

Bordi, I., and A. Sutera, 2001: Fifty years of precipitation: Some spatially remote teleconnnections. *Water Resour. Manage.,* **15,** 247–280, doi:10.1023/A:1013353822381.

Druyan, L. M., 2011: Studies of 21st-century precipitation trends over West Africa. *Int. J. Climatol.,* **31,** 1415–1424, doi:10.1002/joc.2180.

Edwards, D. C., and T. B. McKee, 1997: Characteristics of 20th century drought in the United States at multiple time scales. Colorado State University Dept. of Atmospheric Science Climatology Rep. 97-2/Atmospheric Science Paper 634, 174 pp. [Available online at http://ccc.atmos.colostate.edu/edwards.pdf.]

Goodrich, G. B., and A. W. Ellis, 2006: Climatological drought in Arizona: An analysis of indicators for guiding the governor's Drought Task Force. *Prof. Geogr.,* **58,** 460–469, doi:10.1111/j.1467-9272.2006.00582.x.

Guenang, G. M., and F. Mkankam Kamga, 2012: Onset, retreat and length of the rainy season over Cameroon. *Atmos. Sci. Lett.,* **13,** 120–127, doi:10.1002/asl.371.

Guttman, N. B., 1998: Comparing the Palmer drought index and the standardized precipitation index. *J. Amer. Water Resour. Assoc.,* **34,** 113–121, doi:10.1111/j.1752-1688.1998.tb05964.x.

——, 1999: Accepting the standardized precipitation index: A calculation algorithm. *J. Amer. Water Resour. Assoc.,* **35,** 311–322, doi:10.1111/j.1752-1688.1999.tb03592.x.

Harris, I., P. D. Jones, T. J. Osborn, and D. H. Lister, 2014: Updated high-resolution grids of monthly climatic observations—The CRU TS3.10 dataset. *Int. J. Climatol.,* **34,** 623–642, doi:10.1002/joc.3711.

Hayes, M. J., M. D. Svoboda, D. A. Wilhite, and O. V. Vanyarkho, 1999: Monitoring the 1996 drought using the standardized

precipitation index. *Bull. Amer. Meteor. Soc.,* **80,** 429–438, doi:10.1175/1520-0477(1999)080<0429:MTDUTS>2.0.CO;2.

Kandji, T. S., L. Verchot, and J. Mackensen, 2006: Climate change and variability in the Sahel region: Impacts and adaptation strategies in the agricultural sector. United Nations Environment Programme/World Agroforestry Centre Rep., 48 pp. [Available online at http://www.unep.org/Themes/Freshwater/Documents/pdf/ClimateChangeSahelCombine.pdf.]

Lana, X., C. Serra, and A. Burgueno, 2001: Patterns of monthly rainfall shortage and excess in terms of the standardized precipitation index for Catalonia (NE Spain). *Int. J. Climatol.,* **21,** 1669–1691, doi:10.1002/joc.697.

Livada, I., and V. D. Assimakopoulos, 2007: Spatial and temporal analysis of drought in Greece using the standardized precipitation index (SPI). *Theor. Appl. Climatol.,* **89,** 143–153, doi:10.1007/s00704-005-0227-z.

Lloyd-Hughes, B., and M. A. Saunders, 2002: A drought climatology for Europe. *Int. J. Climatol.,* **22,** 1571–1592, doi:10.1002/joc.846.

Manatsa, D., W. Chingombe, H. Matsikwa, and C. H. Matarira, 2008: The superior influence of Darwin Sea level pressure anomalies over ENSO as a simple drought predictor for southern Africa. *Theor. Appl. Climatol.,* **92,** 1–14, doi:10.1007/s00704-007-0315-3.

McKee, T. B., N. J. Doesken, and J. Kliest, 1993: The relationship of drought frequency and duration to time scales. *Proc. Eighth Conf. of Applied Climatology,* Anaheim, CA, Amer. Meteor. Soc., 179–184.

Mishra, A. K., and V. R. Desai, 2005: Drought forecasting using stochastic models. *J. Stochastic Environ. Res. Risk Assess.,* **19,** 326–339, doi:10.1007/s00477-005-0238-4.

New, M., M. Hulme, and P. Jones, 1999: Representing twentieth-century space–time climate variability. Part I: Development of a 1961–90 mean monthly terrestrial climatology. *J. Climate,* **12,** 829–856, doi:10.1175/1520-0442(1999)012<0829:RTCSTC>2.0.CO;2.

——, ——, and ——, 2000: Representing twentieth-century space–time climate variability. Part II: Development of 1901–96 monthly grids of terrestrial surface climate. *J. Climate,* **13,** 2217–2238, doi:10.1175/1520-0442(2000)013<2217:RTCSTC>2.0.CO;2.

Ntale, H. K., and T. Y. Gan, 2003: Drought indices and their application to East Africa. *Int. J. Climatol.,* **23,** 1335–1357, doi:10.1002/joc.931.

Pal, I., and A. Al-Tabbaa, 2011: Assessing seasonal precipitation trends in India using parametric and non-parametric statistical techniques. *Theor. Appl. Climatol.,* **103,** 1–11, doi:10.1007/s00704-010-0277-8.

Palmer, W. C., 1965: Meteorological drought. U.S. Dept. of Commerce Weather Bureau Research Paper 45, 65 pp. [Available online at http://www.ncdc.noaa.gov/temp-and-precip/drought/docs/palmer.pdf.]

Panahi, H., and S. Asadi, 2011: Estimation of the Weibull distribution based on Type-II censored samples. *Appl. Math. Sci.,* **5,** 2549–2558.

Penlap, K. E., C. Matulla, H. Von Storch, and F. Mkankam Nkamga, 2004: Downscaling of GCM scenarios to assess precipitation changes in the little rainy season (March-June) in Cameroon. *Climate Res.,* **26,** 85–96, doi:10.3354/cr026085.

Quiring, S. M., 2009: Developing objective operational definitions for monitoring drought. *J. Appl. Meteor. Climatol.,* **48,** 1217–1229, doi:10.1175/2009JAMC2088.1.

Ross, S. M., 2009: *Introduction to Probability and Statistics for Engineers and Scientists.* 4th ed. Associated Press, 664 pp.

Seiler, R. A., M. Hayes, and L. Bressan, 2002: Using the standardized precipitation index for flood risk monitoring. *Int. J. Climatol.,* **22,** 1365–1376, doi:10.1002/joc.799.

Stephens, M. A., 1970: Use of the Kolmogorov–Smirnov, Cramér–Von Mises and related statistics without extensive tables. *J. Roy. Stat. Soc.,* **32B,** 115–122. [Available online at http://www.jstor.org/stable/2984408.]

Svoboda, M., and Coauthors, 2002: The Drought Monitor. *Bull. Amer. Meteor. Soc.,* **83,** 1181–1190. [Available online at http://journals.ametsoc.org/doi/abs/10.1175/1520-0477%282002%29083%3C1181%3ATDM%3E2.3.CO%3B2.]

Szalai, S., and C. Szinell, 2000: Comparison of two drought indices for drought monitoring in Hungary—A case study. *Drought and Drought Mitigation in Europe,* J. V. Vogt and F. Somma, Eds., Springer, 161–166.

Tarhule, A., Z. Saley-Bana, and P. J. Lamb, 2009: A prototype GIS for rainfall monitoring in West Africa. *Bull. Amer. Meteor. Soc.,* **90,** 1607–1614, doi:10.1175/2009BAMS2697.1.

Thom, H. C. S., 1958: A note on the gamma distribution. *Mon. Wea. Rev.,* **86,** 117–122, doi:10.1175/1520-0493(1958)086<0117:ANOTGD>2.0.CO;2.

UNEP, 2002: *African Environment Outlook: Past, Present and Future Perspectives.* United Nations Environment Programme, 422 pp. [Available online at http://www.unep.org/dewa/africa/publications/aeo-1/.]

Vicente-Serrano, S. M., 2006: Spatial and temporal analysis of droughts in the Iberian Peninsula (1910-2000). *Hydrol. Sci. J.,* **51,** 83–97, doi:10.1623/hysj.51.1.83.

——, S. Begueria, and J. I. López-Moreno, 2010: A multiscalar drought index sensitive to global warming: The standardized precipitation evapotranspiration index. *J. Climate,* **23,** 1696–1718, doi:10.1175/2009JCLI2909.1.

Wilks, D. S., 1995: *Statistical Methods in the Atmospheric Science: An Introduction.* Academic Press, 467 pp.

——, 2006: *Statistical Methods in the Atmospheric Sciences.* 2nd ed. Academic Press, 627 pp.

Wu, H., M. D. Svoboda, M. J. Hayes, D. A. Wilhite, and F. Wen, 2007: Appropriate application of the standardized precipitation index in arid locations and dry seasons. *Int. J. Climatol.,* **27,** 65–79, doi:10.1002/joc.1371.

Wu, S.-J., 2002: Estimations of the parameters of the Weibull distribution with progressively censored data. *J. Japan Statist. Soc.,* **32,** 155–163, doi:10.14490/jjss.32.155.

Yuan, X., E. F. Wood, N. W. Chaney, J. Sheffield, J. Kam, M. Liang, and K. Guan, 2013: Probabilistic seasonal forecasting of African drought by dynamical models. *J. Hydrometeor.,* **14,** 1706–1720, doi:10.1175/JHM-D-13-054.1.

Zhang, Q., X. Chong-Yu, and Z. Zengxin, 2009: Observed changes of drought/wetness episodes in the Pearl River basin, China, using the standardized precipitation index and aridity index. *Theor. Appl. Climatol.,* **98,** 89–99, doi:10.1007/s00704-008-0095-4.